Lifetime measurements in ^{102}Mo interpreted in the interacting boson model and the X(5) symmetry

C. E. Jones,[1,2,*] A. M. Bruce,[1] D. Reygadas,[1] N. Mărginean,[3] R. Mărginean,[3] C. R. Niță,[3] G. Ağgez,[4] T. Beck,[5,†] M. Boromiza,[3] M. Brunet,[6] R. B. Cakirli,[4,7] R. L. Canavan,[6] A. Chalil,[8,9] C. Clisu,[3] N. Florea,[3] E. R. Gamba,[1] E. Ganioglu,[4] I. Gheorghe,[3] J. P. Greene,[10] K. Hadyńska-Klęk,[11] J. Kleemann,[5] S. Lalkovski,[12] R. Lica,[3] T. J. Mertzimekis,[8] C. Mihai,[3] R. Mihai,[3] A. Mitu,[3] R. Neveling,[13] A. Olacel,[3] A. Oprea,[3] Zs. Podolyák,[6] P. H. Regan,[6,14] L. Sahin,[4] C. Sotty,[3] L. Stan,[3] I. Stiru,[3] S. Toma,[3] A. Turturica,[3] S. Ujeniuc,[3] P. Van Isacker,[15] and A. P. Weaver[1]

[1]*School of Computing, Engineering and Mathematics, University of Brighton, Brighton, Sussex BN2 4GJ, United Kingdom*
[2]*GSI Helmholtzzentrum für Schwerionenforschung GmbH, 64291 Darmstadt, Germany*
[3]*Horia Hulubei National Institute of Physics and Nuclear Engineering (IFIN-HH), R-077125 Bucharest, Romania*
[4]*Department of Physics, Istanbul University, Istanbul 34134, Turkey*
[5]*Institut für Kernphysik, TU Darmstadt, Schlossgartenstraße 9, D-64289 Darmstadt, Germany*
[6]*Department of Physics, University of Surrey, Guildford, Surrey GU2 7XH, United Kingdom*
[7]*Max-Planck-Institut für Kernphysik, Saupfercheckweg 1, D-69117 Heidelberg, Germany*
[8]*Department of Physics, University of Athens, Zografou Campus, GR-15784 Athens, Greece*
[9]*IRFU, CEA, Université Paris-Saclay, 91191 Gif-sur-Yvette, France*
[10]*Physics Division, Argonne National Laboratory, Argonne, Illinois 60439, USA*
[11]*Heavy Ion Laboratory, University of Warsaw, PL 02-093 Warsaw, Poland*
[12]*Faculty of Physics, University of Sofia "St. Kliment Ohridski", Sofia 1164, Bulgaria*
[13]*iThemba LABS, P.O. Box 722, Somerset West 7129, South Africa*
[14]*Department of Medical, Marine and Nuclear, National Physical Laboratory, Teddington TW11 0EB, United Kingdom*
[15]*Grand Accélérateur National d'Ions Lourds, CEA/DRF–CNRS/IN2P3, Boulevard Henri Becquerel, F-14076 Caen, France*

(Received 27 March 2024; revised 23 January 2025; accepted 27 February 2025; published 24 March 2025)

Lifetimes of low-lying excited states in ^{102}Mo populated in the two-neutron transfer reaction ^{100}Mo(^{18}O, ^{16}O) ^{102}Mo were measured using the recoil distance Doppler shift method at the IFIN-HH Tandem accelerator. Lifetimes of the 2_1^+, 0_2^+, 4_1^+, 2_2^+, 2_3^+, 3_1^+, 6_1^+, (0_3^+), 4_2^+, (3_1^-), and (5_1^-) states were obtained. The deduced electromagnetic transition strengths have been compared to calculations performed in the interacting boson model framework including models representing the U(5) and X(5) symmetries. It is found that ^{102}Mo lies between the U(5) limit and the X(5) critical point symmetry.

DOI: 10.1103/PhysRevC.111.034325

I. INTRODUCTION

Composite physical systems such as atoms or nuclei can be characterized by their shape, which is often observed to evolve with particle number. Spherical systems may vibrate, while deformed systems have an additional rotational degree of freedom. For nuclei as their proton Z and neutron N numbers move away from the magic numbers [1] they exhibit strong collective behaviors. Collective excited states can be understood by their relationship to the geometric limits of anharmonic vibrators [2], deformed rotors [3], and γ-soft rotors [4]. In the algebraic framework of the interacting boson model (IBM) these limits are analogous to the dynamical symmetries of the U(6) group: U(5) [5], SU(3) [6], and O(6) [7], respectively. While nuclei rarely conform so strictly to such limits, they provide a useful means of classification.

It is important to study the regions between these limits and in particular the *critical points* in the transition between two limits, where the shape and structure of nuclei evolve most rapidly. Three critical point symmetries have been proposed: E(5) in the transition between the U(5) and O(6) limits [8], and X(5) in the transition between the U(5) and SU(3) limits [9]. There is no critical point between the SU(3) and O(6) limits; however, O(6) itself can be considered as a critical point between prolate and oblate SU(3) [10]. E(5) and X(5) are not dynamic symmetries of the IBM but rather approximate analytical solutions to the Bohr Hamiltonian [3]. The nuclei ^{152}Sm and ^{150}Nd have been suggested as displaying key characteristics of the X(5) critical point symmetry [11,12], and ^{104}Mo has also been proposed as a potential candidate for an X(5) nucleus based on the energy levels of the yrast

*Present address: Department of Physics, University of Surrey, Guildford, Surrey GU2 7XH, United Kingdom.
†Present address: Laboratoire de Physique Corpusculaire Caen, 6 boulevard Maréchal Juin, 14050 Caen Cedex, France.

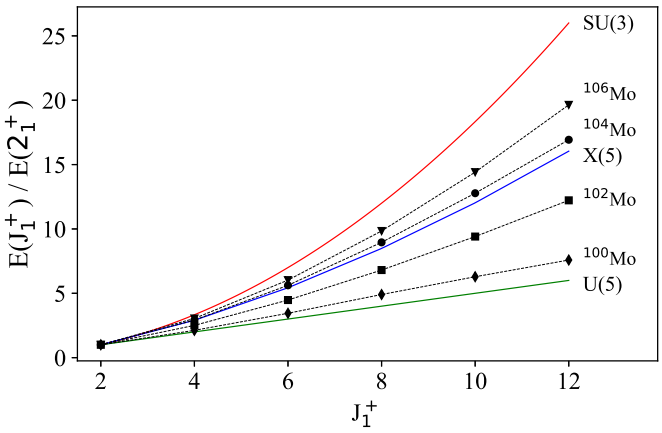

FIG. 1. The energy ratio of yrast band states to the first 2^+ state in ^{106}Mo, ^{104}Mo, ^{102}Mo, and ^{100}Mo, compared with predictions of the U(5) and SU(3) limits, as well as the X(5) symmetry.

band, $K = 2$ and $K = 4$ bands. In their paper, Hutter *et al.* [13] compare the energy ratio of yrast states to the first 2^+ state to the predictions of the U(5) and SU(3) limits as well as that of the X(5) symmetry, for several molybdenum isotopes. Figure 1 shows the details of this comparison and ^{104}Mo is seen to lie very close to the predictions of X(5), and ^{102}Mo is shown to lie roughly midway between the U(5) and X(5) predictions. The purpose of this paper is not to suggest ^{102}Mo as a candidate for X(5) nor U(5), as energy ratio predictions demonstrate that neither mode is entirely suitable. Rather the low-lying structure of ^{102}Mo will be examined and discussed based on both energy levels and newly determined transition strengths, with the U(5) and X(5) symmetries providing useful frameworks for comparison and interpretation.

II. EXPERIMENTAL DETAILS

Excited states in the isotope ^{102}Mo were populated in the two-neutron transfer reaction ^{100}Mo(^{18}O, ^{16}O)^{102}Mo. A 50 MeV beam of ^{18}O, delivered by the 9 MV FN Pelletron Tandem Accelerator at the Horia Hulubei National Institute of Physics and Nuclear Engineering (IFIN-HH), Măgurele, Romania, was impinged upon a self-supported target of 1.0 mg cm^{-2} isotopic (>99% enrichment) ^{100}Mo. For the duration of the experimental run the beam current was kept to between 5 and 10 pnA. The target and a 5 mg cm^{-2} ^{197}Au stopper were mounted at the center of the ROmanian array for SPectroscopy in HEavy ion REactions (ROSPHERE) [14]. ROSPHERE was used in a configuration consisting of 25 high-purity germanium (HPGe) detectors Compton suppressed with bismuth germanate shields, arranged in five rings of five detectors each, at angles of 37° (forward, "FW"), 70°, 90°, 110°, and 143°(backward, "BW"). Each HPGe detector is positioned at a slightly different target-to-detector distance based on its position in the array and the type of detector used; these distances range between 176 and 217 mm. The germanium array was coupled with a plunger device, accommodating a target-stopper range of $10 - 2000\,\mu$m, to allow for recoil distance Doppler shift (RDDS) measurements. Data were recorded at eight distances of 11.7, 15.5, 26, 36, 50, 75, 150, and 250 μm, for acquisition periods of between 8 h (250 μm) and 95 h (36 μm). The data acquisition system was triggered by at least two Compton-suppressed HPGe detectors firing in coincidence. In conjunction with the HPGe detectors, an array of silicon solar cell detectors named SORCERER [15,16] was mounted inside the ROSPHERE target chamber, with the intention of providing some particle selectivity for cleaner γ-ray spectra. A schematic of SORCERER is illustrated in Fig. 2; the solar cells were arranged at backward angles with respect to the beam axis (between 130.4° and 165.5°) and provide approximately 11% solid angle coverage.

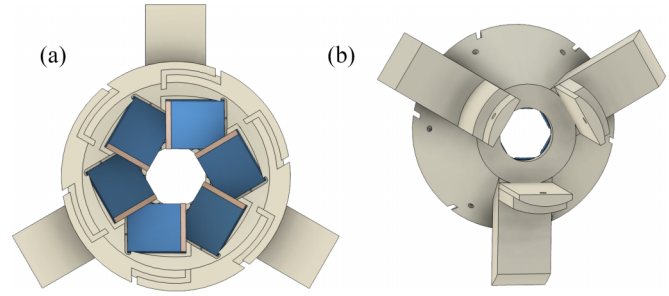

FIG. 2. Two views of the 3D-printed solar cell mount, part of the SORCERER array [15]. Solar cells are represented by the blue squares on the left-hand image. When mounted in ROSPHERE, the side displaying the solar cells faces the beam direction.

The velocity of the recoiling ^{102}Mo nuclei was determined by measuring the energies of the shifted and unshifted components of the most intense transitions ($0_2^+ \to 2_1^+$, $4_1^+ \to 2_1^+$, and $2_2^+ \to 2_1^+$), yielding $v/c = 1.78(5)\%$. A particle energy spectrum detected by the solar cells is shown in Fig. 3(a). Two main regions are identified. The leftmost region contains mostly recoils from Coulomb excitation on the Au stopper. The rightmost region marked with red gate markers contains the recoils of interest: the ^{16}O produced in the two-neutron transfer reaction, as well as a number of additional recoils such as ^{18}O from the Coulex of the ^{100}Mo target and ^{14}C from the α-transfer reaction producing ^{104}Ru. Figures 3(b) and 3(c) display two projections of a γ-γ coincidence matrix: in the top panel no coincidence with the observation of a charged particle with the solar cells is enforced; in the bottom panel this condition is required. The total counts are reduced by a factor of almost 20; however, the spectra are much cleaner if coincidences with the detection of charged particles are enforced. Reaction products from fusion are completely suppressed, while the transitions of interest in ^{102}Mo are enhanced relative to contaminant transitions from the Coulomb excitation of the ^{197}Au stopper. Transitions in ^{100}Mo and ^{104}Ru in particular remain strong since these recoils cannot be distinguished in the solar cell energy spectrum.

III. ANALYSIS

A. Level scheme

The level scheme of ^{102}Mo has been constructed using γ-γ coincidence analysis. In total 24 γ-ray transitions were identified, belonging to 14 excited energy states. Transitions and levels are summarized in Table I and the level scheme is

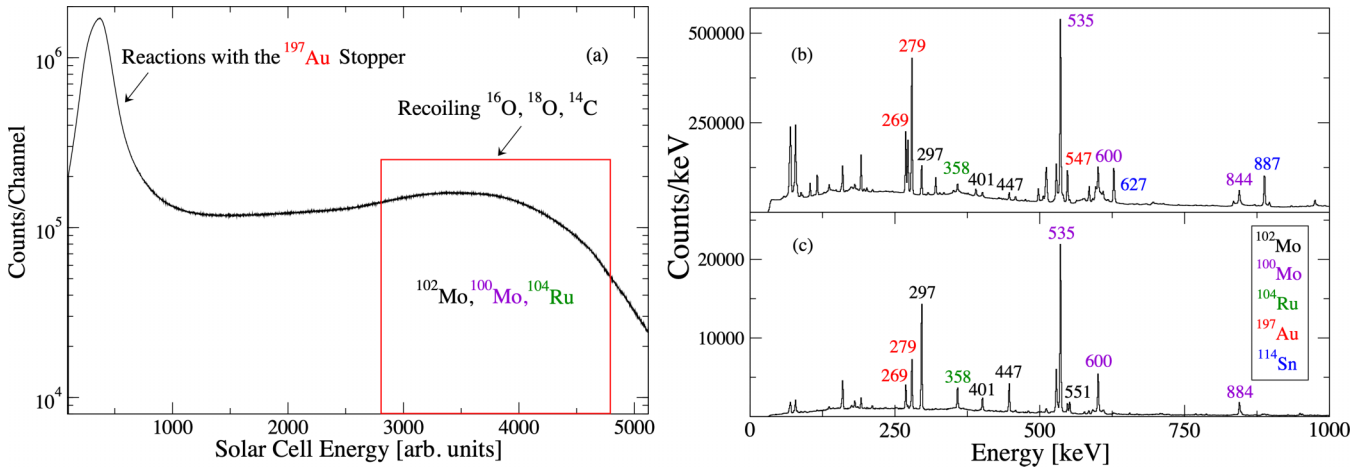

FIG. 3. (a) An energy spectrum for the (summed) six solar cell detectors. The left-hand region represents particles backscattered after reactions with the gold stopper. In the right-hand region nuclei such as ^{16}O and ^{18}O scattered by the ^{102}Mo and ^{100}Mo, respectively, are included. [(b), (c)] Projections of a γ-γ matrix produced from coincidences in all detectors at a target-stopper distance of 11 μm. In the top spectrum no solar cell coincidence condition is enforced; in the bottom spectrum the gate indicated by the red box in (a) has been imposed. The most intense transitions are labeled by their nucleus in each panel.

TABLE I. γ-ray energies, relative transition intensities (I_γ), and branching ratios (BRs) observed in the ^{100}Mo(^{18}O, ^{16}O)^{102}Mo reaction. Intensities are normalized to the $2_1^+ \rightarrow 0_g^+$ transition. Energy levels are determined using a least-squares adjustment to the γ-ray energies [17].

	This work					Previous works
E_{level} (keV)	$J_i^\pi \rightarrow J_f^\pi$	E_γ (keV)	E_f (keV)	I_γ	BR	BR [18,19]
296.1(1)	$2_1^+ \rightarrow 0_g^+$	296.1(1)	0	100(3)	100	100
697.3(2)	$0_2^+ \rightarrow 2_1^+$	401.1(2)	296.1	16.5(10)	100	100
743.4(1)	$4_1^+ \rightarrow 2_1^+$	447.2(4)	296.1	28.3(16)	100	100
847.8(1)	$2_2^+ \rightarrow 2_1^+$	551.8(2)	296.1	16.1(93)[a]	100(18)[b]	100(5)
	$2_2^+ \rightarrow 0_g^+$	847.5(2)	0	11.5(56)[c]	71(22)[b]	58(6)
1245.1(1)	$3_1^+ \rightarrow 2_2^+$	397.0(3)	847.8	1.5(4)	35(9)	19(4)
	$3_1^+ \rightarrow 2_1^+$	949.0(1)	296.1	4.4(4)	100(9)	100(11)
1249.6(1)	$2_3^+ \rightarrow 4_1^+$	506.1(3)	743.4	1.4(2)	49(9)	25(13)
	$2_3^+ \rightarrow 0_2^+$	552.6(1)	697.3	$\leqslant 3.4$	$\leqslant 116$	50(13)
	$2_3^+ \rightarrow 2_1^+$	953.2(2)	296.1	2.9(4)	100(12)	100(25)
	$2_3^+ \rightarrow 0_g^+$	1249.9(4)	0	0.9(4)	32(13)	75(25)
1327.9(2)	$6_1^+ \rightarrow 4_1^+$	584.6(1)	743.4	6.8(9)	100	100
1328.2(1)	$(0_3^+) \rightarrow 2_2^+$	480.5(7)	847.8	2.2(3)	100	
	$(0_3^+) \rightarrow 2_1^+$	1031.9(2)	296.1	0.9(4)	42(21)	
1398.3(2)	$4_2^+ \rightarrow 2_2^+$	550(2)	847.8	$\leqslant 1.3$	$\leqslant 68$	94(5)
	$4_2^+ \rightarrow 4_1^+$	654.8(2)	743.4	1.9(4)	100	100(7)
	$4_2^+ \rightarrow 2_1^+$	1102.5(3)	296.1	1.2(4)	65(25)	44(11)
1616.3(2)	$\rightarrow 2_3^+$	367.3(5)	1249.6	[d]	[d]	78(22)
	$\rightarrow 2_1^+$	1320.0(2)	296.1	1.1(3)	100	100(22)
1746.8(5)	$\rightarrow 4_1^+$	1003.5(5)	743.4	$\leqslant 0.4$	100	100(21)
1868.0(6)	$\rightarrow 3_1^+$	622.9(6)	1245.1	$\leqslant 0.02$	100[e]	39(9)
1875.7(5)	$(3_1^-) \rightarrow 4_1^+$	1132.9(6)	743.4	1.8(7)	100(37)	
	$(3_1^-) \rightarrow 2_1^+$	1578.8(7)	296.1	1.0(5)	57(36)	
2148.6(3)	$(5_1^-) \rightarrow 4_1^+$	1405.3(2)	743.4	1.1(3)	100	100

[a]Determined using the branching ratio relative to the 847.5 keV transition.
[b]Obtained by gating on the 480.5 keV feeding transition ($(0_3^+) \rightarrow 2_2^+$).
[c] Determined by subtracting the contribution from the overlapping 844 keV transition in ^{100}Mo. The intensity of the 844 was calculated from the observed intensity of the 1372 keV transition depopulating the same 3^- state and the known branching ratio [20].
[d]Unable to distinguish from contaminant transition in ^{100}Mo.
[e]Previously reported transitions [18] at 1021.9 and 1126.1 keV are not observed in these data (see text for details).

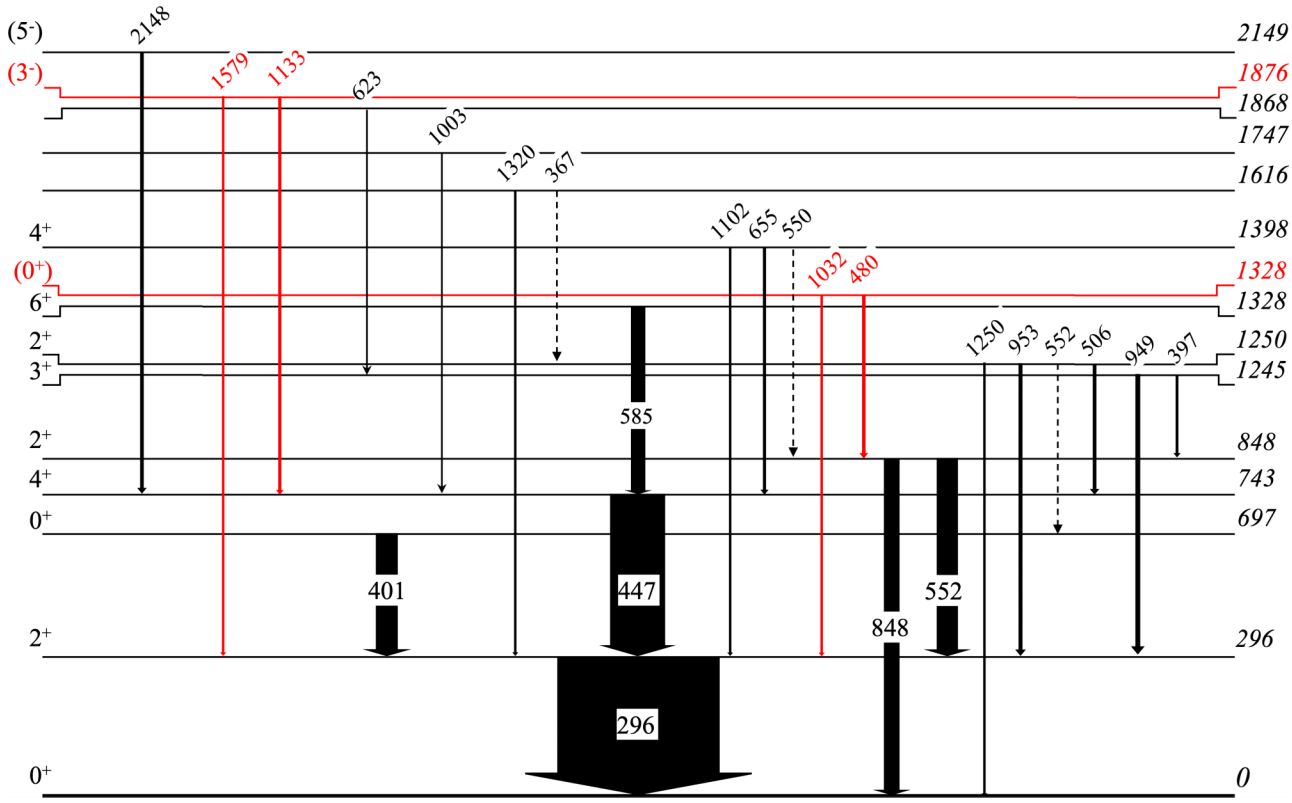

FIG. 4. The ^{102}Mo level scheme constructed from transitions observed in this work. Arrows are proportional to the intensities reported in Table I and energies are rounded to the nearest keV. Dotted arrows represent transitions for which the intensity could not be determined. In red are new transitions and excited states. Level energies have been determined using a least-squares technique on the γ-ray energies [17], and spins and parities are adopted from Ref. [21].

presented in Fig. 4. In addition to the 296.1 keV transition from the first excited state there are two other transitions observed to decay directly to the ground state: depopulating the 2_2^+ state at 847.8 keV and the 2_3^+ state at 1249.6 keV. Otherwise all other transitions eventually feed the 2_1^+ state.

The measured branching ratios presented in column 6 of Table I are generally in good agreement with literature, with most found to be consistent within one standard deviation. The 397.0 keV transition deexciting the 3_1^+ state at 1245.1 keV and the 506.1 and 1249.9 keV transitions exciting the 2_3^+ state are consistent within two standard deviations. A major exception is the 622.9 keV transition, a single transition observed in this work to depopulate an excited state at 1868.0 keV and hence reported with a branching ratio of 100. A study by Gietz *et al.* [18] reports on a more intense transition at 1021.9 keV and gives a branching ratio of 39% for the 622.9 keV transition; however, the 1021.9 keV is not observed in the present work. Of additional note are the branching ratios of the transitions with energies between 550 and 553 keV. Three transitions with energies of 550, 551.8, and 552.6 keV overlap and intensities cannot be measured directly. The intensity of the 550 keV transition has been determined by scaling to the 480.5 keV transition in a spectrum gated on the 847.5 keV transition, which depopulates the 2_2^+ state. Both the 550 and 480.5 keV transitions feed the 2_2^+ state directly. The intensity of the 552.6 keV transition has been determined by scaling to the 953.2 keV transition (which depopulates the same level) in a spectrum gated on the 367.3 keV transition. Since these gated spectra will still capture a small intensity of the overlapping 551.8 keV transition, the I_γ and branching ratios are reported as upper limits. The intensity of the 551.8 keV transition was determined with a multistep calculation that begins with a measurement of the intensity of the 1372 keV transition in ^{100}Mo. The branching ratio between this transition and the 844 keV transition depopulating the same 3^- state is known [20] and was used to calculate the intensity of the 844 keV transition which overlaps with the 847.5 keV transition of ^{102}Mo. The intensity of the 844 keV transition was subtracted from the total to obtain the intensity of the 847.5 keV transition, and then the I_γ of the 551.8 keV transition can be calculated using the branching ratio determined in a spectrum gated on the 480.5 keV transition. Since there are multiple steps of subtraction and multiplication the uncertainties accumulate, resulting in large error bars on the I_γ of the 551.8 and 847.5 keV transitions.

Details of two excited states which have been observed in γ spectroscopy for the first time are discussed in the following sections.

1. The 1328.2 keV state

Figure 5 presents evidence for the first observation of γ rays depopulating the (0_3^+) state. In Fig. 5(a) an energy gate is illustrated placed across the 551.8 keV transition ($2_2^+ \rightarrow 2_1^+$)

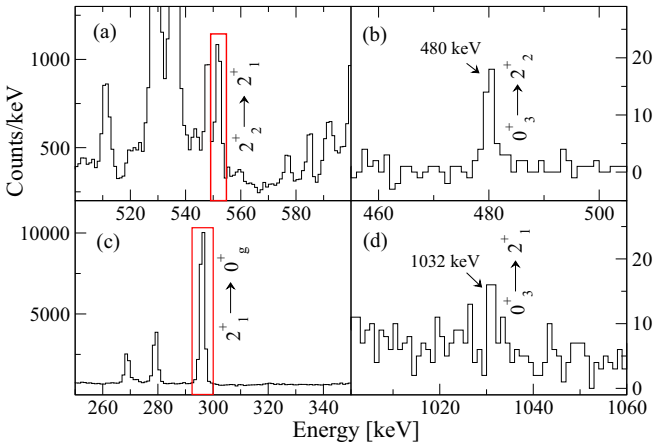

FIG. 5. γ-ray spectra produced from a γ-γ matrix, constructed from coincidences measured in 90° detectors at all target-stopper distances. Energy gates are marked with a red box and energies are rounded to the nearest keV. (a) A projection centered on the 551.8 keV transition ($2_2^+ \rightarrow 2_1^+$). (b) A gated spectrum produced with the energy gate displayed in (a), centered on the 480.5 keV transition ($(0_3^+) \rightarrow 2_2^+$). (c) A projection centered on the 296.1 keV transition ($2_1^+ \rightarrow 0_g^+$). A gated spectrum produced with the energy gate displayed in (c), centered on the 1031.9 keV transition ($(0_3^+) \rightarrow 2_1^+$).

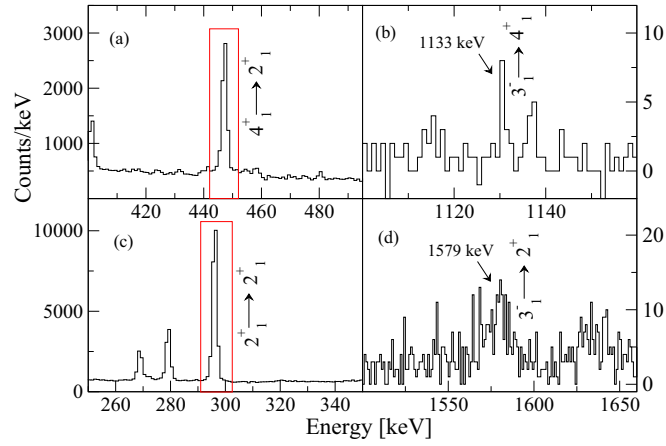

FIG. 6. γ-ray spectra produced from a γ-γ matrix, constructed from coincidences measured in 90° detectors at all target-stopper distances. Energy gates are marked with a red box and energies are rounded to the nearest keV. (a) A projection centered on the 447.2 keV transition ($4_1^+ \rightarrow 2_1^+$). (b) A gated spectrum produced with the energy gate displayed in (a), centered on the 1132.9 keV transition ($(3_1^-) \rightarrow 4_1^+$). (c) A projection centered on the 296.1 keV transition ($2_1^+ \rightarrow 0_g^+$). (d) A gated spectrum produced with the energy gated displayed in (c), centered on the 1578.8 keV transition ($(3_1^-) \rightarrow 2_1^+$).

in the projection of a γ-γ matrix, and Fig. 5(b) displays the resultant gated spectrum centered on the 480.5 keV transition ($(0_3^+) \rightarrow 2_2^+$). In Fig. 5(c) an energy gate is illustrated across the 296.1 keV transition ($2_1^+ \rightarrow 0_g^+$) in the projection of the coincidence matrix, while Fig. 5(d) shows the resultant gated spectrum centered on the 1031.9 keV transition ($(0_3^+) \rightarrow 2_1^+$). The 551.8 keV transition depopulates an excited state at 847.8 keV, and thus transitions illustrated in each row of Fig. 5 sum to an excited state at approximately the same energy, around 1328 keV. In γ-energy spectra produced by gating on the 480.5 keV transition only peaks at 296.1, 551.8, and 847.8 keV are observed, and after gating on the 1031.9 keV transition only the 296.1 keV transition is observed in the resultant spectrum. Since the 480.5and 1031.9 keV transitions both feed 2^+ states, they cannot originate from the known 6_1^+ state at 1327.9 keV, as such transitions would both have to be $E4$ or $M5$ in nature, which are strongly suppressed in comparison to $E2$ transitions. The energy of this state is consistent with the excited state measured at 1334(5) keV, revealed to be a 0^+ state with angular distribution measurements performed by Casten *et al.* [22]. Furthermore, a 0_3^+ state would complete the quintuplet of states resultant from the three-quadrupole-phonon interactions predicted by the vibrational model of the nucleus and the U(5) limit of the IBM. These are the first observations of both the 480.5 and 1031.9 keV γ rays, and hence the first observation of this likely 0_3^+ state via γ-ray spectroscopy.

2. The 1875.7 keV state

Figure 6 presents the first evidence of γ rays depopulating the (3_1^-) state. In Fig. 6(a) an energy gate is illustrated placed across the 447.2 keV transition ($4_1^+ \rightarrow 2_1^+$) in the projection of a γ-γ matrix, while Fig. 6(b) displays the resultant gated spectrum centered on a transition at 1132.9 keV ($(3_1^-) \rightarrow 4_1^+$). In Fig. 6(c) an energy gate is illustrated across the 296.1 keV transition ($2_1^+ \rightarrow 0_g^+$) in the γ-γ matrix projection, and Fig. 6(d) shows the resultant gated spectrum centered on the 1578.8 keV transition ($(3_1^-) \rightarrow 2_1^+$). The 447.2 keV transition depopulates an excited state at an energy of 743.4 keV, and thus the transitions in each row of Fig. 6 sum to a state at approximately the same energy, around 1876 keV. By gating on the 1132.9 keV transition, a γ-ray energy spectrum is obtained containing only the 447.3 and 296.1 keV transitions. Additionally, after gating on the 1578.8 keV transition, only the 296.1 keV transition is observed. Thus, these two transitions can be confidently placed in the level scheme. Proton angular distribution measurements performed by Rahman and Chowdhury [23] following the ^{100}Mo(t,p) ^{102}Mo reaction indicate a 3^- state at 1878(2) keV, meaning the 1132.9 and 1578.8 keV transitions observed in these data are consistent with the first γ-ray spectroscopy observations of a (3_1^-) state at 1875.7 keV.

B. Lifetimes

When a nucleus decays in flight between the target and stopper, emitted γ rays are Doppler shifted according to

$$E = E_0 \frac{\sqrt{1-\beta^2}}{1-\beta\cos\theta}, \tag{1}$$

where E is the observed γ-ray energy, E_0 is the energy of the emitted γ ray, β is the velocity v of the nucleus relative to c, and θ is the angle of emission. As the target-stopper distance x is increased, the ratio between the intensity of unshifted γ

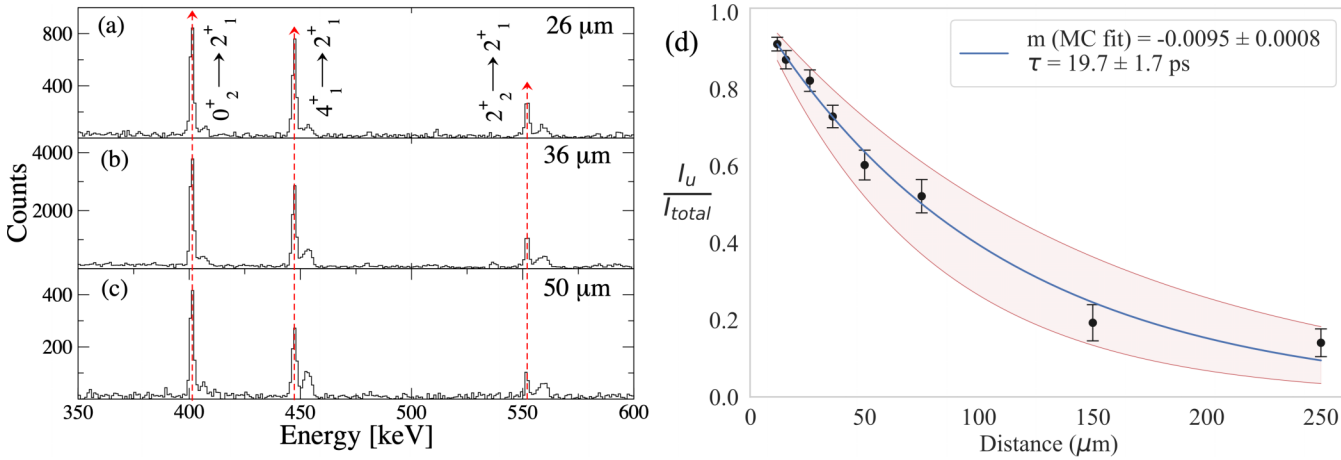

FIG. 7. [(a)–(c)] From left to right: the 401.1 keV transition ($0_2^+ \rightarrow 2_1^+$), 447.2 keV transition ($4_1^+ \rightarrow 2_1^+$), and 551.8 keV transition ($2_2^+ \rightarrow 2_1^+$), observed in gated spectra with an energy gate on the 296.1 keV transition ($2_1^+ \rightarrow 0_g^+$) at distances of 26, 36, and 50 μm. (d) The decay curve for the 4_1^+ state measured using the 447.2 keV transition ($4_1^+ \rightarrow 2_1^+$) observed in the FW ring of detectors.

rays, I_u, and of γ rays shifted according to Eq. (1), I_s, changes exponentially:

$$\frac{I_u}{I_u + I_s} = \exp\left(-\frac{x}{v\tau}\right), \tag{2}$$

where τ is the mean lifetime of the origin state. This effect is illustrated in Figs. 7(a)–7(c), where the transitions $0_2^+ \rightarrow 2_1^+$, $4_1^+ \rightarrow 2_1^+$, and $2_2^+ \rightarrow 2_1^+$ are shown at distances of 26, 36, and 50 μm. For the 2_1^+ state it was possible to measure the lifetime by gating from above in the level scheme, on the shifted component of the $4_1^+ \rightarrow 2_1^+$ transition. Gating on the shifted component of a directly feeding transition has the advantage of the lifetime measurement being unaffected by side feeding. For every other lifetime measured, statistics were insufficient to gate on a feeding transition; energy gates were placed below in the level scheme and hence contributions from side feeding can affect the value determined with Eq. (1). The results presented do not account for these contributions, but a general discussion is given in Sec. III B 5.

The value of a lifetime and its uncertainty were determined using a Monte Carlo fitting routine. For each distance x_i, a corresponding value for the ratio of unshifted intensity to total intensity (labeled y_i) is generated from a normal distribution $\mathcal{N}(y_i, \delta y_i)$. A weighted least-squares fit is performed on this set of points to determine the decay constant m, related to the lifetime of the state by

$$m = -\frac{1}{v\tau}, \tag{3}$$

where v is the velocity of the nucleus (1.78% of c as previously discussed). This procedure is repeated 10^5 times, producing a distribution of possible m values from which a mean and standard deviation can be obtained. Measurements were made in both the FW and BW rings of ROSPHERE and hence weighted average values are presented for each state lifetime. Figure 7(d) illustrates an example of a Monte Carlo fit for a measurement of the 4_1^+ lifetime using the 447.2 keV transition ($4_1^+ \rightarrow 2_1^+$) measured in the FW ring. The mean lifetimes of 11 excited states are shown in column 2 of Table II.

1. Analysis of the 2_1^+ state

The 2_1^+ state decays via a single 296.1 keV transition to the ground state. The evolution of the unshifted and shifted components of this transition with distance was observed by gating above on the shifted component of the 447.2 keV ($4_1^+ \rightarrow 2_1^+$) transition, over the greatest four distances. A lifetime of $\tau_{2_1^+} = 175(75)$ ps was measured. This value is in agreement with previous measurements of 180(6) ps [24], $186.9^{+18.3}_{-18.7}$ ps [25], and 150(10) ps [26]. The uncertainty in the measurement presented is fairly large since the distances used in the current work were chosen to target significantly shorter lifetimes.

2. Analysis of the 0_2^+, 4_1^+, and 2_2^+ states

For the 0_2^+ state, the 401.1 keV transition ($0_2^+ \rightarrow 2_1^+$) was used to determine the lifetime. The weighted average of $\tau_{0_2^+} = 41(5)$ ps is consistent with a previous RDDS measurement for this state of 40(16) ps [24] within a single standard deviation. A more recent measurement of 33(4) ps [26] is consistent within two standard deviations.

The 4_1^+ state lifetime was measured using the 447.2 keV transition ($4_1^+ \rightarrow 2_1^+$). A lifetime of $\tau_{4_1^+} = 19(1)$ ps was obtained, consistent with a previous RDDS measurement of 18(4) ps [24] and Doppler shift attenuation method measurement of $27.8^{+10.5}_{-8.3}$ ps [25] within one standard deviation. A more recent RDDS measurement gives a lifetime of 15.9(12) ps [26], which is not consistent with this work within 1σ. A possible reason for this inconsistency may be due to the feeding considerations Esmaylzadeh *et al.* have used in their determination of the lifetime, a consideration that is also discussed in Sec. III B 5 in this work.

The 551.8 keV transition ($2_2^+ \rightarrow 2_1^+$) was used to measure the lifetime of the 2_2^+ state. This state also decays via a 847.5 keV transition ($2_2^+ \rightarrow 0_g^+$), although this could not be used as it is obscured by the intense 845 keV transition ($(3_1^-) \rightarrow 2_2^+$) of ^{100}Mo. A weighted average of $\tau_{2_2^+} = 13(2)$ ps is close but inconsistent within 1σ with the only previous measurement giving the lifetime as 10.3(12) ps [26].

TABLE II. The lifetime of excited states measured in this work, and reduced transition probabilities calculated from these lifetimes and the transition energies and branching ratios listed in Table I. $B(E2)$ values are given in W.u., $B(M1)$ values are given in $10^{-4}\mu_N^2$, and $B(E1)$ values are given in 10^{-5} W.u. Where lifetimes have large uncertainties, transition strengths are given with asymmetrical uncertainties.

	This work					τ (ps), previous works		
E_{level}	τ (ps)	$J_i^\pi \to J_f^\pi$	$B(E2)\downarrow$	$B(M1)\downarrow$	$B(E1)\downarrow$	Ref. [24]	Ref. [25]	Ref. [26]
296.1	175(75)	$2_1^+ \to 0_g^+$	70^{+50}_{-20}			180(6)	$186.9^{+18.3}_{-18.7}$	150(10)
697.3	41(5)	$0_2^+ \to 2_1^+$	68(8)			40(16)		33(4)
743.4	19(1)	$4_1^+ \to 2_1^+$	85(4)			18(4)	$27.8^{+10.5}_{-8.3}$	15.9(12)
847.8	13(2)	$2_2^+ \to 2_1^+$	25(5)[a]	$3.0^{+1.3}_{-1.5}$[a]				10.3(12)
		$2_2^+ \to 0_g^+$	2.1(5)					
1245.1	9.2(17)	$3_1^+ \to 2_2^+$	$\leqslant 82(22)$[b]	$\leqslant 254(69)$[b]				$5.5^{+1.0}_{-3.5}$
		$3_1^+ \to 2_1^+$	3.0(6)[c]	$0.7^{+0.6}_{-0.4}$[c]				
1249.6	7.1(15)	$2_3^+ \to 4_1^+$	20(4)					
		$2_3^+ \to 0_2^+$	31(5)					
		$2_3^+ \to 2_1^+$	$\leqslant 1.8(3)$[b]	$\leqslant 31(4)$[b]				
		$2_3^+ \to 0_g^+$	0.14(3)					
1327.9	5.1(8)	$6_1^+ \to 4_1^+$	83(13)				3.2(7)	$6.7^{+0.7}_{-3.1}$
1328.2	3.8(8)	$(0_3^+) \to 2_2^+$	210^{+70}_{-50}					
		$(0_3^+) \to 2_1^+$	1.9(8)					
1398.3	7.2(16)	$4_2^+ \to 2_2^+$	24(6)					< 4
		$4_2^+ \to 4_1^+$	12(3)[d]	24(4)[d]				
		$4_2^+ \to 2_1^+$	0.67(19)					
1875.7	2.9(5)	$(3_1^-) \to 4_1^+$			6.8(20)			
		$(3_1^-) \to 2_1^+$			1.4(6)			
2148.6	6.0(42)	$(5_1^-) \to 4_1^+$			2.7^{+63}_{-11}			

[a] An $M1/E2$ mixing ratio of $7.0^{+1.8}_{-0.6}$ was used [27].
[b] Assumed to be at the limits of pure $M1$ or $E2$ transitions.
[c] An $M1/E2$ mixing ratio of -9^{+2}_{-3} was used [27].
[d] An $M1/E2$ mixing ratio of 2^{+3}_{-1} was used [27].

3. *Analysis of the* 3_1^+, 2_3^+, 6_1^+, (0_3^+), *and* 4_2^+ *states*

The 3_1^+ lifetime was measured using the 949.0 keV transition ($3_1^+ \to 2_1^+$). This state has a second transition at 397.0 keV ($3_1^+ \to 2_2^+$); however, the statistics for this decay were too poor to observe the evolution of unshifted vs shifted intensities at a range of distances. Additionally components from the 397.0 keV transition and components from the 401.1 keV transition ($0_2^+ \to 2_1^+$) overlap with one another. A weighted average of $\tau_{3_1^+} = 9.2(17)$ ps is inconsistent with the only previous measurement of $5.5^{+1.0}_{-3.5}$ ps [26]. A possible reason for this discrepancy is that in Ref. [26] Esmaylzadeh *et al.* did not consider the 2_3^+ state, which decays via a 953.2 keV transition ($2_3^+ \to 2_1^+$). The 949.0 and 953.2 keV transitions are close enough in energy that the measurement of the intensity of one may be impacted if the other is not considered, i.e., if they are not fitted as two overlapping Gaussian peaks.

The 953.2 keV transition ($2_3^+ \to 2_1^+$) was used to determine the lifetime of the 2_3^+ state. Two additional transitions were observed to originate from this state; however, the statistics for both the 506.1 keV transition ($2_3^+ \to 4_1^+$) and 552.6 keV transition ($2_3^+ \to 0_2^+$) were too few to measure across multiple distances. A weighted average of $\tau_{2_3^+} = 7.1(15)$ ps was determined.

For the 6_1^+ state the 584.6 keV transition ($6_1^+ \to 4_1^+$) was used to measure the lifetime. A weighted average of $\tau_{6_1^+} = 5.1(8)$ ps was measured. This value is not consistent within 1σ of a previous measurement of 3.2(7) ps by Ralet *et al.* [25]. A more recent measurement by Esmaylzadeh *et al.* [26] gives a value of $6.7^{+0.7}_{-3.1}$ ps, which is consistent within uncertainties, depending on the level of feeding assumed.

The (0_3^+) state was observed to decay via two transitions: the 480.5 keV ($(0_3^+) \to 2_2^+$) and the 1031.9 keV ($(0_3^+) \to 2_1^+$). Both transitions were used for a measurement of the lifetime of this state; however, statistics were only significant enough when measured in the BW ring. A weighted average of $\tau_{(0_3^+)} = 3.8(8)$ ps was measured.

For the 4_2^+ state the 654.8 keV transition ($4_2^+ \to 4_1^+$) was used to determine the lifetime. This state decays via a second transition at 1102.5 keV ($4_2^+ \to 2_1^+$); however, the statistics were too poor for a measurement of the lifetime. A weighted average of $\tau_{4_2^+} = 7.2(16)$ ps was measured. This is not consistent with the only previous measurement of <4 ps, which may be due to the authors' [26] simulation of feeding from above in the level scheme, which is not accounted for in this work.

4. *Analysis of the* (3_1^-) *and* (5_1^-) *states*

The 1579 keV transition ($(3_1^-) \to 2_1^+$) was used in the measurement of the (3_1^-) lifetime. A second transition at 1132.9 keV ($(3_1^-) \to 4_1^+$) was observed; however, statistics were insufficient to obtain a lifetime measurement. A weighted average of $\tau_{(3_1^-)} = 2.9(5)$ ps was determined.

A single measurement for the lifetime of the (5_1^-) state was made, using the 1405.3 keV transition $((5_1^-) \rightarrow 4_1^+)$ observed in the BW ring, as statistics in the FW ring were insignificant from the background. A value of $\tau_{(5_1^-)} = 6.0(42)$ ps was measured.

5. Side-feeding considerations

Side-feeding effects are not observed when gating from above in the level scheme, and thus the 2_1^+ state is not considered in this section. From the γ-ray intensities measured in this work, the largest side-feeding contributions are those to the 0_2^+, 4_1^+, and 2_2^+ states. Using a modified version of the procedure detailed by Stan and Clisu [28], Monte Carlo simulations were performed to determine the lifetimes of the 0_2^+, 4_1^+, and 2_2^+ excited states, considering contributions from the 2_3^+ state for the 0_2^+ lifetime, contributions from the 6_1^+, 2_3^+, 4_2^+, (3_1^-), and (5_1^-) state for the 4_1^+ lifetime, and contributions from the 4_2^+, (0_3^+), and 3_1^+ states for the 2_2^+ lifetime. Lifetimes were input to the code using the results in Table II, and population ratios were calculated by considering the relative γ-ray intensities into and out of each excited state, given in Table I. In the case of the 550 and 552.6 keV transitions populating the 2_2^+ and 0_2^+ levels, respectively, the maximum γ-ray intensities of 1.3 and 3.4 were input to the simulation. The lifetime calculations were simulated 10^6 times each, after which the results $\tau_{0_2^+} = 38.9(99)$ ps, $\tau_{4_1^+} = 17.2(23)$ ps, and $\tau_{2_2^+} = 11.9(31)$ ps were obtained.

The side feeding shifts each lifetime shorter, as expected, pushing the 4_1^+ and 2_2^+ states into agreement at the level of 1σ with the result of Esmaylzadeh *et al.* [26]. The 0_2^+ lifetime is also reduced, and is in fact in agreement with the work of Esmaylzadeh *et al.*; however, this is primarily due to the large uncertainty introduced. The only additional feeding effects which were not included in the simulation are from the 622.9 and 367.3 keV transitions; however, low statistics made it impossible to measure the lifetimes of their respective states, and hence these contributions are not considered. Since it is not possible to determine a full picture of the feeding effects, calculations of the transition strengths in the following section use only the values presented in Table II.

IV. DISCUSSION

A. Level energies

Since neither the U(5) limit nor the X(5) symmetry is suitable for the description of the energy levels of ^{102}Mo (see Fig. 1), it is worthwhile to introduce a more general IBM Hamiltonian [29] in order to capture as much detail of the nucleus as possible:

$$\hat{H}_{\rm IBM} = \epsilon n_d + a_0 \hat{P}^\dagger \hat{P} + a_1 \hat{L}\cdot\hat{L} + a_2 \hat{Q}\cdot\hat{Q} + a_3 \hat{T}_3\cdot\hat{T}_3 + a_4 \hat{T}_4\cdot\hat{T}_4, \quad (4)$$

where $\hat{n}_d$ is the d-boson number operator, $\hat{P}^\dagger$ is the boson pairing operator, $\hat{P}^\dagger = s^\dagger s^\dagger + d^\dagger\cdot d^\dagger$, $\hat{L}_\mu$ is the angular momentum operator, $\hat{L}_\mu = \sqrt{10}(d^\dagger\tilde{d})^{(1)}_\mu$, $\hat{Q}_\mu$ is the quadrupole operator, $\hat{Q}_\mu = (s^\dagger\tilde{d} + d^\dagger s)^{(2)}_\mu + \chi(d^\dagger\tilde{d})^{(2)}_\mu$, and $\hat{T}_\lambda = (d^\dagger\tilde{d})^{(\lambda)}_\mu$. The coefficients ϵ and a_{0-4} as well as χ are treated as free parameters. With the fortran program *fiti* [30], Eq. (4) is used to generate a set of energy levels while minimizing the root-mean-square error ($\Delta E_{\rm RMS}$) between a calculated scheme and experimental values by adjusting the free parameters. The first nine excited states (up to the 4_2^+ state at 1398.3 keV) are used, since negative-parity states cannot be generated in IBM-1. At the U(5) limit Eq. (4) reduces to

$$\hat{H}_{\rm U(5)} = \epsilon n_d + a_1 \hat{L}\cdot\hat{L} + a_3 \hat{T}_3\cdot\hat{T}_3 + a_4 \hat{T}_4\cdot\hat{T}_4. \quad (5)$$

Similarly, this equation is used to generate a level scheme for the first nine excited states. Parameters for each resultant Hamiltonian are given in Table III. In the fit of the general IBM Hamiltonian $\hat{H}_{\rm IBM}$ to the nine states in ^{102}Mo the parameters a_3 and a_4 do not lead to a lower value of the $\Delta E_{\rm RMS}$ and can be kept to zero. Likewise, the parameter χ in $\hat{H}_{\rm IBM}$ is ill determined from energies. An optimum value of $\chi = -1.02$ is found in the $E2$ operator (see below), which is also used in the Hamiltonian.

TABLE III. Level-energy-optimized Hamiltonian parameters, in units of keV.

$\hat{H}$	ϵ	a_0	a_1	a_2	a_3	a_4
$\hat{H}_{\rm U(5)}$	0.5		12.5		54.8	98.4
$\hat{H}_{\rm IBM}$	523.9	22.2	8.8	−12.7		

An interesting result from the fit with the general Hamiltonian $\hat{H}_{\rm IBM}$ is the requirement for a nonzero pairing contribution (a_0). As a nucleus moves from the U(5) vertex of the Casten triangle [31], along the U(5)-SU(3) edge toward the X(5) critical point, an increase in the quadrupole term (a_2) is expected. However, an increase in the pairing term is introduced as a nucleus becomes more γ soft, moving toward the O(6) vertex of the triangle. This γ softness has been investigated in ^{102}Mo previously by Esmaylzadeh *et al.*, who did indeed find signatures of γ softness in their reduced transition probabilities calculations [26]. The X(5) energy eigenvalue equation used to generate a best-fit level scheme is

$$E(s, L, n_\gamma, K) = E_0 + B(x_{s,\nu})^2 + A(n_\gamma + 1), \quad (6)$$

where $x_{s,\nu}$ is the sth zero of the Bessel function $J_\nu(x)$, with

$$\nu = \left[\frac{L(L+1) - K^2}{3} + \frac{9}{4}\right]^{1/2}. \quad (7)$$

Excitation energies are independent of E_0 and depend only on A and B in Eq. (6), which are treated as free parameters. The L values in a sequence (n_γ, s) are determined by K; for $K = 0$, $L = 0, 2, 4, \ldots$ and for $K \neq 0$, $L = K, K+1, K+2, \ldots$. The values of K are determined by n_γ which takes the values $0, 1, 2, \ldots$; for $n_\gamma = 0$, $K = 0$, for $n_\gamma = 1$, $K = \pm 2$, for $n_\gamma = 2$, $K = 0, \pm 4$, etc.

In order to make a comparison with X(5), it must be determined which states belong to the $n_\gamma = 0$ bands and which belong to the $n_\gamma = 1$ band. There are a number of possible configurations in which excited states in ^{102}Mo could be assigned and here we consider two: either $2^+_{n_\gamma=1,s=1}$ is the 2_3^+ state at 1249.6 keV [labeled X(5)$_1$] or it is the 2_2^+ state at 847.8 keV [labeled X(5)$_2$]. These two choices are illustrated

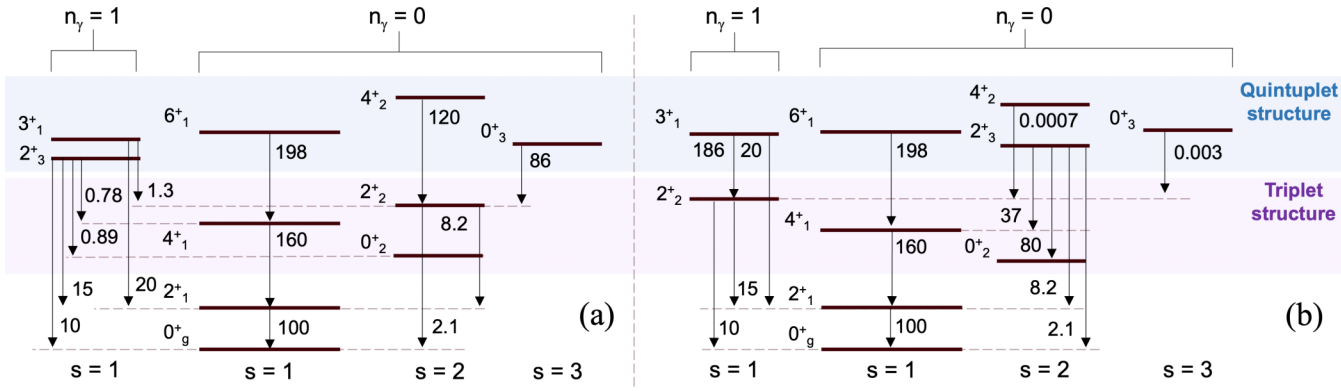

FIG. 8. Two X(5) configurations of excited states in ^{102}Mo. (a) The $2^+_{n_\gamma=1,s=1}$ state is the 2^+_3 (measured at 1249.6 keV). (b) The $2^+_{n_\gamma=1,s=1}$ state is the 2^+_2 (measured at 847.8 keV). Strengths of $\Delta K = 0$ transitions are normalized to $B(E2; 2^+_1 \to 0^+_g) = 100$ while those of $\Delta K = 2$ transitions are normalized to $B(E2; 2^+_{n_\gamma=1,s=1} \to 0^+_g) = 10$. Level energies are not to scale.

in Fig. 8. Transition strengths at the X(5) critical point are calculated based on the quantum numbers n_γ, s, and L; pertinent transition strengths that change with these quantum numbers are therefore labeled in this figure. In addition, the $4^+_{n_\gamma=1,s=1}$ could be considered to be the 4^+_2 level at 1398.3 keV, as in Ref. [26], but this is not done here. The optimal parameters for X(5)$_1$ as they pertain to Eq. (6) are (in keV) $A = 1146.76$ and $B = 17.45$, giving $\Delta E_{\rm RMS} = 337$. The optimal parameters for X(5)$_2$ are (in keV) $A = 939.86$ and $B = 18.48$, giving $\Delta E_{\rm RMS} = 362$.

The energy-optimized level schemes for each model are depicted in Fig. 9. The first nine excited states of ^{102}Mo exhibit a recognizably U(5)-like structure, with the signature pattern of a 2^+ state, followed by a $0^+, 2^+, 4^+$ triplet, followed by a $0^+, 2^+, 3^+, 4^+, 6^+$ quintuplet. It is no surprise that the U(5) model fits the states in ^{102}Mo quite well, with a $\Delta E_{\rm RMS} = 47$ keV, although the model is not able to correctly order the states in the triplet and quintuplet structures, indicating at least one additional parameter is required to resolve the discrepancy. Both X(5) schemes are unable to fit the yrast band to the correct scale, which is a consequence of attempting a simultaneous fit of the $s = 1$, 2, and 3 bands; adjusting the scale parameter B to better fit the yrast band results in much higher energy $0^+_2, 2^+_2, 4^+_2$, and 0^+_3 states. Additionally, the X(5)$_2$ scheme is unable to move the $2^+_{n_\gamma=1,s=1}$ below the $2^+_{n_\gamma=0,s=2}$ state. The Hamiltonian $\hat{H}_{\rm IBM}$ by comparison provides a closer fit to the experimental energies, with $\Delta E_{\rm RMS} = 26$ keV, although it should be noted even in this model the 2^+_3 and 3^+_1 states are ordered incorrectly.

B. Transition strengths

In this section $E2$ transition strengths are calculated with the parametrizations obtained previously from the fits to level energies. The transition strengths measured in this work can be found in columns 4–6 of Table II. The intensities of the 550 and 552.6 keV transitions were taken to be at their maximum.

(E2) transition strengths

Table IV compares experimental and calculated $B(E2)$ values. Some of the $E2$ transitions have rather large uncertainties that should be included in the assessment of the performance of the different models. In order to do so, we define the dimensionless quantity

$$\sigma(E2) = \left[\frac{1}{N}\sum_{i=1}^{N}\left(\frac{B(E2)_i^{\rm expt} - B(E2)_i^{\rm theo}}{B(E2)_i^{\rm unc}}\right)^2\right]^{1/2}, \qquad (8)$$

TABLE IV. Comparison of experimental $B(E2)$ values in ^{102}Mo with results obtained with the U(5), with two X(5) models, and with a general Hamiltonian of the IBM.

	$B(E2)$				
$J_i^\pi \to J_f^\pi$	Expt.	U(5)	X(5)$_1$	X(5)$_2$	IBM
$2^+_1 \to 0^+_g$	70^{+50}_{-20}	22	49	21	45
$4^+_1 \to 2^+_1$	85(4)	40	79	34	74
$6^+_1 \to 4^+_1$	83(13)	52	97	42	87
$0^+_2 \to 2^+_1$	68(8)	40	31	13	43
$2^+_2 \to 0^+_g$	2.1(5)	0	1.0	1.8	0.73
$2^+_2 \to 2^+_1$	25(5)	40	4.0	2.7	26
$4^+_2 \to 2^+_1$	0.67(19)	0	0.46	0.20	0.04
$4^+_2 \to 4^+_1$	12(3)	25	3.0	1.3	15
$4^+_2 \to 2^+_2$	24(6)	27	59	5×10^{-5}	36
$(0^+_3) \to 2^+_1$	1.9(8)	0	0.29	0.12	0.09
$(0^+_3) \to 2^+_2$	210^{+70}_{-50}	52	42	4×10^{-3}	27
$2^+_3 \to 0^+_g$	0.14(3)	0	0.20	0.44	0.24
$2^+_3 \to 4^+_1$	20(4)	18	0.01	7.7	14
$2^+_3 \to 0^+_2$	31(5)	24	0.02	17	28
$3^+_1 \to 2^+_1$	3.0(6)	0	0.31	3.5	1.4
		$\sigma(E2)$			
Triplet transitions		6.43	3.41	7.63	2.49
Quintuplet transitions		3.11	3.73	4.24	2.21
All transitions		4.19	3.52	5.25	2.22

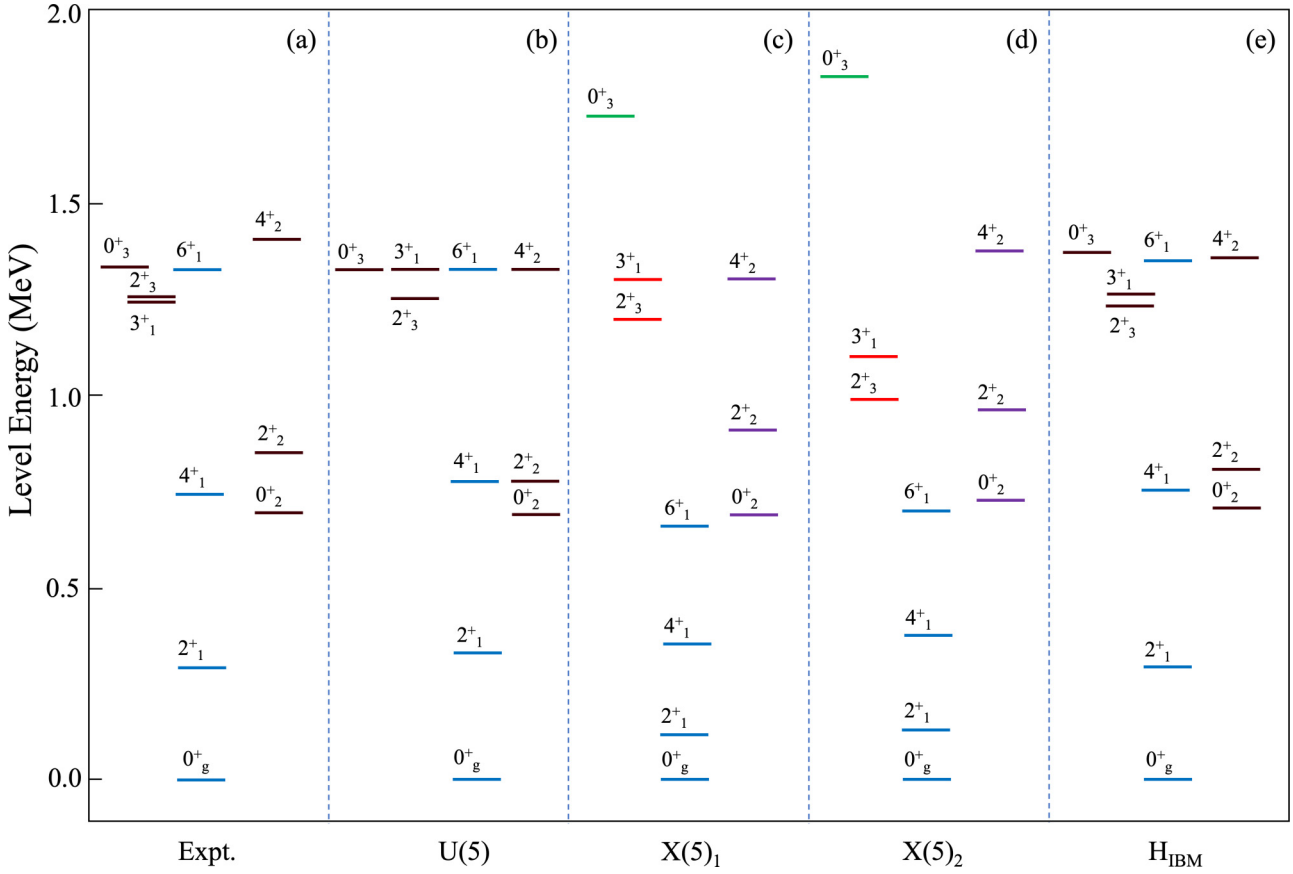

FIG. 9. The first nine excited states in ^{102}Mo. From left to right: (a) Measured values in this work, calculated level schemes using (b) the U(5) Hamiltonian, [(c), (d)] the X(5) Hamiltonians, and (e) the general IBM Hamiltonian. Energies are to scale; however, close gaps (<10 keV) have been slightly exaggerated for readability. Blue lines belong to the yrast band. In X(5) members of the $n_\gamma = 0$, $s = 2$ band are purple, of the $n_\gamma = 0$, $s = 3$ bandare green, and of the $n_\gamma = 1$, $s = 1$ band are red.

where the sum runs over the N available experimental $B(E2)$ values. Each of the four models contains one or two parameters in the $E2$ operator to be adjusted to minimize $\sigma(E2)$. The two $B(E2)$ values for transitions where the mixing ratio is not known and hence only an upper limit can be provided are not considered in this minimization: these are the $2^+_3 \to 2^+_1$ and $3^+_1 \to 2^+_2$ transitions.

In the consistent-Q formalism of the IBM [32] the $E2$ operator is taken as

$$e_b \hat{Q}_\mu = e_b\left[(s^\dagger \tilde{d} + d^\dagger s)^{(2)}_\mu + \chi (d^\dagger \tilde{d})^{(2)}_\mu\right], \tag{9}$$

where $\hat{Q}_\mu$ is the quadrupole operator of the Hamiltonian and e_b is the boson effective charge. In the U(5) limit the quadrupole operator does not appear in Hamiltonian (5) and the $E2$ transitions are independent of χ. The fitted boson effective charge is found to be $e_b^2 = 1.58^2$ W.u. If the general IBM Hamiltonian $\hat{H}_{IBM}$ of Eq. (4) is used, $E2$ transitions depend on both parameters e_b and χ, and a best fit is obtained for $\chi = -1.02$, as previously discussed, and $e_b^2 = 1.56^2$ W.u.

In the geometric collective model $E2$ transition rates are obtained from the matrix elements of the operator

$$t\beta\left(\mathcal{D}^{(2)}_{\mu 0}(\theta_i)\cos\gamma + \frac{1}{\sqrt{2}}\left[\mathcal{D}^{(2)}_{\mu 2} + \mathcal{D}^{(2)}_{\mu -2}\right]\sin\gamma\right), \tag{10}$$

where β and γ are the quadrupole shape parameters and $\mathcal{D}^{(2)}_{\mu\mu'}(\theta_i)$ are Wigner $\mathcal{D}$ functions in terms of the three Euler angles θ_i. The X(5) model assumes a harmonic potential $\frac{1}{2}\omega^2\gamma^2$, which can be solved analytically in the limit of small oscillations in γ (i.e., of large ω). The reduced $E2$ transition rates can then be written as

$$B(E2; n_\gamma sKL \to n'_\gamma s'K'L') = (LK2K' - K|L'K')^2 \times \left(\frac{A_{n_\gamma n'_\gamma}}{J_{\nu+1}(x_{s\nu})J_{\nu'+1}(x_{s'\nu'})}\int_0^1 y^2 J_\nu(x_{s\nu}y)J_{\nu'}(x_{s'\nu'}y)dy\right)^2, \tag{11}$$

where the symbol $(\cdot\cdot|\cdot)$ is a Clebsch-Gordan coefficient. In line with the discussion of Bijker *et al.* [33], the coefficients $A_{n_\gamma n'_\gamma}$ can be expressed in terms of $t\beta_W$, where β_W is the infinite-wall parameter in the β potential, and of the parameter $b \equiv (\omega\sqrt{\langle\beta^2\rangle})^{-1/2}$ in the γ potential. The first few $A_{n_\gamma n'_\gamma}$ coefficients are found to be

$$A_{00} \approx A_{11} \approx 2t\beta_W, \quad A_{10} = \frac{\sqrt{2}}{3}t\beta_W b^3, \tag{12}$$

in the limit of small b. The results in Table IV are obtained with the best-fit parameters (in W.u.) $A^2_{00} = A^2_{11} = 51.77^2$ and $A^2_{10} = 2.930^2$ in X(5)$_1$ and $A^2_{00} = A^2_{11} = 33.82^2$ and $A^2_{10} = 9.929^2$ in X(5)$_2$.

There is a clear hierarchy in the performance of the four models. The calculation with the general IBM Hamiltonian has a lower average $\sigma(E2)$ deviation as compared to the $X(5)_1$, which in turn outperforms U(5) and $X(5)_2$. The U(5) calculation is particularly deficient in the description of the triplet transitions, which is in marked difference for the quintuplet transitions. In contrast, the calculation with the general IBM Hamiltonian performs consistently across all transitions, albeit with a deviation over two. A similar remark applies to the comparison of $X(5)_1$ and $X(5)_2$, only the former having similar $\sigma(E2)$ deviations for triplet and quintuplet transitions. With an analysis based on average $\sigma(E2)$ deviations, problems for specific transitions should be kept in mind. For example, while $X(5)_1$ leads to acceptable results for most transitions, it fails completely to predict the $B(E2; 2_3^+ \rightarrow 4_1^+)$ and $B(E2; 2_3^+ \rightarrow 0_2^+)$ values. In fact, none of the models is able to predict the correct ratio of these two $B(E2)$ values.

Concerning X(5) analysis it should be emphasized that it is based on the assumption of small γ oscillations around $\gamma = 0$, that is, of a large restoring force ω or a small b parameter. Equation (12) and the fitted values of the coefficients $A_{n_\gamma n'_\gamma}$ allow one to obtain an estimate, leading to $b \approx 0.62$ for $X(5)_1$ and $b \approx 1.07$ for $X(5)_2$. While the first value might be consistent with the assumption of small b, the second is certainly not.

V. CONCLUSION

The (0_3^+) and (3_1^-) excited states have been observed with γ-ray spectroscopy for the first time. The lifetimes of the 2_1^+, 0_2^+, 4_1^+, 2_2^+, 3_1^+, 2_3^+, 6_1^+, (0_3^+), 4_2^+, (3_1^-), and (5_1^-) states have been determined with RDDS measurements. $B(E2)$, $B(M1)$, and $B(E1)$ strengths have been determined where appropriate using measured lifetimes and branching ratios, and mixing ratios from the literature where necessary.

Comparisons of the experimental excited state energies and $B(E2)$ values with IBM calculations support the suggestion illustrated in Fig. 1, that ^{102}Mo may be a nucleus lying somewhere between the U(5) limit and the X(5) critical point, but not precisely at either. While $B(E2)$ values can be reasonably suited to an X(5) scheme, dependent on the quantum number selection, X(5) is severely limited in its ability to generate excited state energies, failing completely for this nucleus. Conversely the U(5) limit is well suited to predict the quasivibrational level scheme of ^{102}Mo, but does not perform particularly well when calculating transition strengths. It is important to note that the U(5) model does much better with the quintuplet state $B(E2)$ values than those of the triplet states, which may be an indicator of competing shapes coexisting in the nuclear structure. Most interestingly, the general Hamiltonian $\hat{H}_{\rm IBM}$ performs the best in all areas, providing reasonable predictions for both the level energies and $B(E2)$ values. The requirement for a nonzero pairing term in the Hamiltonian may suggest an element of axial deformation. Both shape coexistence and axial deformation have been investigated in the study by Esmaylzadeh *et al.* [26]. Further research into the 3^- and 5^- lifetimes in the surrounding nuclear region is needed to elucidate the nature of the negative-parity states in ^{102}Mo.

ACKNOWLEDGMENTS

The author C.E.J. would like to thank the Science & Technology Facility Council for funding his Ph.D. studentship. The authors A.M.B., E.R.G., and A.P.W. acknowledge the support from STFC Grant No. ST/P003982. Authors from the University of Surrey acknowledge the support from Grants No. ST/V001108/1 and No. ST/P005314/1. The work of N.F. was supported by a grant of the Ministry of Research, Innovation and Digitization, CNCS/CCCDI – UEFISCDI, Project No. PN-III-P1-1.1-TE-2019-0337, within PNCDI III. The author S.L. acknowledges financial support from the European Union – Next Generation EU, the National Recovery and Resilience Plan of the Republic of Bulgaria, Project No. BG-RRP-2.004-0008-C01. R.B.C. acknowledges support from the Max-Planck Partner group. All the authors are grateful to the ROSPHERE and SORCERER collaborations for providing the equipment used for the measurements presented in this work.

[1] O. Haxel, J. H. D. Jensen, and H. E. Suess, Phys. Rev. **75**, 1766 (1949).
[2] G. Scharff-Goldhaber and J. Weneser, Phys. Rev. **98**, 212 (1955).
[3] A. Bohr, Dan. Mat. Fys. Medd. **26**, 9 (1952).
[4] L. Wilets and M. Jean, Phys. Rev. **102**, 788 (1956).
[5] A. Arima and F. Iachello, Ann. Phys. **99**, 253 (1976).
[6] A. Arima and F. Iachello, Ann. Phys. **111**, 201 (1978).
[7] A. Arima and F. Iachello, Ann. Phys. **123**, 468 (1979).
[8] F. Iachello, Phys. Rev. Lett. **85**, 3580 (2000).
[9] F. Iachello, Phys. Rev. Lett. **87**, 052502 (2001).
[10] J. Jolie, R. F. Casten, P. von Brentano, and V. Werner, Phys. Rev. Lett. **87**, 162501 (2001).
[11] R. F. Casten and N. V. Zamfir, Phys. Rev. Lett. **87**, 052503 (2001).
[12] R. Krücken, B. Albanna, C. Bialik, R. F. Casten, J. R. Cooper, A. Dewald, N. V. Zamfir, C. J. Barton, C. W. Beausang, M. A. Caprio *et al.*, Phys. Rev. Lett. **88**, 232501 (2002).
[13] C. Hutter, R. Krücken, A. Aprahamian, C. J. Barton, C. W. Beausang, M. A. Caprio, R. F. Casten, W.-T. Chou, R. M. Clark, D. Cline *et al.*, Phys. Rev. C **67**, 054315 (2003).
[14] D. Bucurescu, I. Căta-Danil, G. Ciocan, C. Costache, D. Deleanu, R. Dima, D. Filipescu, N. Florea, D. Ghiţă, T. Glodariu *et al.*, Nucl. Instrum. Methods Phys. Res., Sect. A **837**, 1 (2016).
[15] T. Beck, C. Costache, R. Lică, N. Mărginean, C. Mihai, R. Mihai, O. Papst, S. Pascu, N. Pietralla, C. Sotty *et al.*, Nucl. Instrum. Methods Phys. Res., Sect. A **951**, 163090 (2020).
[16] T. Beck, C. Costache, R. Lică, N. Mărginean, C. Mihai, R. Mihai, O. Papst, S. Pascu, N. Pietralla, C. Sotty *et al.* (2020), https://github.com/TB-IKP/SORCERER.
[17] GTOL (2013), https://www-nds.iaea.org/public/ensdf_pgm/.

[18] H. Gietz, N. Kaffrell, G. Menzen, and K. Sistemich, Univ. Mainz Ann. Report (unpublished), p. 10.
[19] S. Lalkovski, S. Ilieva, A. Minkova, N. Minkov, T. Kutsarova, A. Lopez-Martens, A. Korichi, H. Hübel, A. Görgen, A. Jansen *et al.*, Phys. Rev. C **75**, 014314 (2007).
[20] G. Molnár, I. Diószegi, Á. Veres, and M. Sambataro, Nucl. Phys. A **403**, 342 (1983).
[21] D. De Frenne, Nucl. Data Sheets **110**, 1745 (2009).
[22] R. Casten, E. Flynn, O. Hansen, and T. Mulligan, Nucl. Phys. A **184**, 357 (1972).
[23] M. A. Rahman and M. S. Chowdhury, Phys. Rev. C **73**, 054311 (2006).
[24] H. Bohn, P. Kienle, D. Proetel, and R. L. Hershberger, Z. Phys. A **274**, 327 (1975).
[25] D. Ralet, S. Pietri, T. Rodríguez, M. Alaqeel, T. Alexander, N. Alkhomashi, F. Ameil, T. Arici, A. Ataç, R. Avigo *et al.* (for the PreSPEC and PreSPEC and AGATA Collaborations), Phys. Rev. C **95**, 034320 (2017).
[26] A. Esmaylzadeh, V. Karayonchev, K. Nomura, J. Jolie, M. Beckers, A. Blazhev, A. Dewald, C. Fransen, R.-B. Gerst, G. Häfner *et al.*, Phys. Rev. C **104**, 064314 (2021).
[27] J. M. Eldridge, B. Fenker, J. H. Hamilton, C. Goodin, C. J. Zachary, E. Wang, A. V. Ramayya, A. V. Daniel, G. M. Ter-Akopian, Y. Ts. Oganessian *et al.*, Eur. Phys. J. A **54**, 15 (2018).
[28] L. Stan and C. Clisu, UPB Sci. Bull. Ser. A **82**, 263 (2020).
[29] A. Arima and F. Iachello, *The Interacting Boson Model* (Cambridge University Press, Cambridge, UK, 1987).
[30] P. Van Isacker (private communication).
[31] R. F. Casten, *Nuclear Structure from a Simple Perspective* (Oxford University Press, Oxford, UK, 1990).
[32] D. D. Warner and R. F. Casten, Phys. Rev. Lett. **48**, 1385 (1982).
[33] R. Bijker, R. F. Casten, N. V. Zamfir, and E. A. McCutchan, Phys. Rev. C **68**, 064304 (2003).